



**FULL PAPER**

Applied  
Organometallic  
Chemistry

**WILEY**

# Cellulose stabilized $\text{Fe}_3\text{O}_4$ and carboxylate-imidazole and Co-based MOF growth as an exceptional catalyst for the Knoevenagel reaction

Elham Zare | Zahra Rafiee

Department of Chemistry, Yasouj University, Yasouj, 75918-74831, Iran

**Correspondence**

Zahra Rafiee, Department of Chemistry, Yasouj University, Yasouj, 75918-74831, Iran.  
Email: z.rafiee@yu.ac.ir;  
zahrarafiee2004@yahoo.com

**Funding information**

Yasouj University, Grant/Award Number: Gryu-89131307

In this study,  $\text{Fe}_3\text{O}_4$  nanoparticles were functionalized with cellulose, and then hybridized with cobalt (II)-based metal-organic framework (Co-MOF) containing carboxylate and imidazole functionalities. FTIR, XRD, FE-SEM, TEM, BET, EDX, VSM and STA analyses were used to characterize the synthesized samples. The resultant  $\text{Fe}_3\text{O}_4$ /cellulose/Co-MOF nanocomposite was applied efficiently as a powerful and economic heterogeneous catalyst in the condensation of a variety of different aromatic aldehydes with malononitrile under solvent-free conditions at room temperature for 10 min and offered the corresponding coupling products in high yields. The catalyst could be straightforwardly separated by a magnet from the reaction mixture and reused without a noteworthy drop in catalytic activity at least five times. The use of  $\text{Fe}_3\text{O}_4$ /cellulose/Co-MOF catalyst outcomes under mild reaction conditions in very short reaction time, outstanding catalytic activity, high recyclability and an easy work-up process for Knoevenagel condensation.

**KEY WORDS**

cellulose,  $\text{Fe}_3\text{O}_4$  nanoparticles, Knoevenagel reaction, metal-organic framework, nanocomposite

## 1 | INTRODUCTION

Metal oxides nanostructures are especially of interest because of their fascinating and unique properties.<sup>[1–8]</sup> Among these metal oxides, the magnetic iron oxide ( $\text{Fe}_3\text{O}_4$ ) nanoparticles are of huge attention, owing to their low cost, easy preparation, and high magnetic permeability and various applications in diverse fields such as catalysis, adsorption, and optoelectronics.<sup>[9–13]</sup> Nevertheless, the application of these nanoparticles is limited by their instability in alkaline and acidic media and easy aggregation, due to high surface free energy, specific surface area, and easy oxidation.<sup>[14]</sup> To overcome these drawbacks, a variety of modification approaches were attempted via adding various materials during or after the construction process to enhance the stability, dispersibility, biodegradability, and biocompatibility of  $\text{Fe}_3\text{O}_4$

nanoparticles.<sup>[15]</sup> So far, diverse materials such as silanes,<sup>[16]</sup> activated carbon<sup>[17]</sup> and biocompatible polymers<sup>[18]</sup> have been efficiently utilized to modify  $\text{Fe}_3\text{O}_4$  nanoparticles. Among these modifiers, cellulose as a bio-polymer has attracted substantial attention owing to its biodegradability, biocompatibility, and outstanding thermal properties. Therefore, cellulose can be utilized as an effective coating material for  $\text{Fe}_3\text{O}_4$  nanoparticles to yield environmentally friendly, biocompatible, and exciting biopolymer-based nanocomposites.<sup>[19–21]</sup>

Metal-organic frameworks (MOFs) are an attractive class of porous crystalline materials that have attracted substantial attention owing to their unique and valuable properties, such as extraordinary surface area, outstanding porosity, order crystalline structures, adjustable surface features, and tunable pore sizes.<sup>[22–24]</sup> These exciting properties of MOFs have led to their applications

in various fields including gas storage, separation, ion exchange, chemical sensors, supercapacitors, medicinal and catalysis.<sup>[25–31]</sup> Nevertheless, the application of these materials has been restricted because of their chemical instability to aqueous and organic media, and strongly acidic or alkaline environment and difficult recovery.<sup>[32]</sup> Recently, MOF-based composites have been fabricated through hybridizing MOFs with other materials, such as metal nanoparticles,<sup>[33]</sup> polymers,<sup>[34,35]</sup> other MOFs<sup>[36]</sup> and COFs,<sup>[37]</sup> which display new properties that are superior to those of the individual components by the combination of features of two ingredients. The composites containing magnetic metal oxides and MOFs displayed magnetic characteristics and large specific surface area, making them excellent candidates for the catalysts of organic reactions.<sup>[38]</sup>

Knoevenagel reaction is accomplished via the condensation of the carbonyl compounds and activated methylene linkages catalyzed by weak bases and acids to form unsaturated compounds.<sup>[39–43]</sup> This condensation reaction has led to the production of significant organic intermediates that are adjustable to different synthetic transformations and biologically significant compounds such as heterocycles,<sup>[44]</sup> carbohydrates<sup>[45]</sup> and drugs.<sup>[46]</sup> Various catalysts including Lewis acids, zeolites, and different amines have been utilized to catalyze the Knoevenagel reaction.<sup>[47–49]</sup> Recently, the various solid-supported heterogeneous catalysts have been applied to Knoevenagel reaction including Hf (IV) MOF,<sup>[50]</sup> metal-coordinated, resorcin[4]arene-based molecular trimer,<sup>[51]</sup> GO-supported PdNi nanoparticles,<sup>[52]</sup> Zn-based MOF,<sup>[53]</sup> amino-functionalized Zn/Cd-MOFs,<sup>[54]</sup> Cu (II)-based metal-organic macrocycle and framework,<sup>[55]</sup> covalent organic frameworks (COFs)<sup>[56]</sup> and Core-Shell MOF/COF.<sup>[57]</sup>

In the present work, Fe<sub>3</sub>O<sub>4</sub>/cellulose/Co-MOF was hydrothermally prepared and utilized as an efficient and cost-effective heterogeneous catalyst for the Knoevenagel reaction under solvent-free conditions. The synergistic effects of Fe<sub>3</sub>O<sub>4</sub> and Co-MOF based on 1,4-benzene dicarboxylate and imidazole are expected to enhance catalytic performance.

## 2 | EXPERIMENTAL

### 2.1 | Materials

The reagents and chemicals including iron (II) chloride tetrahydrate (FeCl<sub>2</sub>.4H<sub>2</sub>O), iron (III) chloride hexahydrate (FeCl<sub>3</sub>.6H<sub>2</sub>O), ammonium hydroxide (NH<sub>4</sub>OH, 25%), sodium hydroxide (NaOH), urea (CO(NH<sub>2</sub>)<sub>2</sub>), cobalt (II) nitrate hexahydrate (Co(NO<sub>3</sub>)<sub>2</sub>.6H<sub>2</sub>O), 1,4-

benzenedicarboxylic acid (1,4-BDC, terephthalic acid), imidazole (IM), N,N-dimethylformamide (DMF), ethanol, benzaldehyde, malononitrile, 4-nitrobenzaldehyde, 4-chlorobenzaldehyde, 2-chlorobenzaldehyde, 4-methoxybenzaldehyde, 4-methylbenzaldehyde, 2-hydroxybenzaldehyde were purchased from Merck Company (Darmstadt, Germany) and used without further purification. Cellulose (Cellulose powder, Cotton linters), fibers, (medium) was supplied by Sigma Company (Milwaukee, WI, USA).

### 2.2 | Apparatus

FT-IR spectra were recorded with a Jasco-680 spectrometer (Tokyo, Japan) in the range of 4000–400 cm<sup>-1</sup>. FT-IR spectra of all compounds were collected by making their pellets in KBr as a medium. The X-ray diffraction patterns of the prepared materials were recorded in the reflection mode using a Bruker, D8 Advance diffractometer. The ultrasonic bath (Tecno-GAZ SPA Ultrasonic system, Italy) was used at a frequency of 60 Hz and power of 130 W. The surface morphology of samples was studied by scanning electron microscopy (SEM; EM10C-ZEISS, 80 KV, Zeiss Co., Germany) and transmission electron microscopy (TEM, EM10C-ZEISS, Zeiss Co., Germany). Nitrogen adsorption/desorption isotherm was measured by Brunauer–Emmett–Teller analysis (Belsorp Mini II, Japan).

### 2.3 | Preparation of Fe<sub>3</sub>O<sub>4</sub> nanoparticles

The Fe<sub>3</sub>O<sub>4</sub> nanoparticles were synthesized by the coprecipitation method<sup>[58]</sup> as follows: FeCl<sub>3</sub>.6H<sub>2</sub>O (0.81 g) and FeCl<sub>2</sub>.4H<sub>2</sub>O (0.3 g) were dissolved in distilled water (25 ml) with stirring at room temperature. Then, ammonia solution (25%, 1.5 ml) was added dropwise into the reaction mixture with stirring at 80 °C under a nitrogen atmosphere and stirred at 80 °C for 1 hr. The resultant precipitate was collected by an external magnet and thoroughly washed with deionized water and dried at 70 °C under vacuum.

### 2.4 | Preparation of Fe<sub>3</sub>O<sub>4</sub>/cellulose nanocomposite

Fe<sub>3</sub>O<sub>4</sub> nanoparticles (0.15 g) were dispersed in 30 mL of an aqueous solution containing NaOH (7 wt.%) and urea (12 wt.%) and cooled to –12 °C for 1 hr. Then, cellulose (0.1 g) was added into the reaction mixture with stirring for 15 min. After freezing for 1 hr, the cellulose was dissolved fully. Then, deionized water was added into the mixture and the Fe<sub>3</sub>O<sub>4</sub>/cellulose nanocomposite was produced. The resultant nanocomposite was collected by an

external magnet and washed with deionized water and dried at 70 °C under vacuum.

## 2.5 | Synthesis of Fe<sub>3</sub>O<sub>4</sub>/cellulose/Co-MOF

Fe<sub>3</sub>O<sub>4</sub>/cellulose (0.2 g) was dispersed in DMF (60 mL) and sonicated for 20 min to dissolve completely. Consequently, a mixture of Co (NO<sub>3</sub>)<sub>2</sub>·6H<sub>2</sub>O (0.87 g, 3 mmol), 1,4-BDC (0.49 g, 3 mmol) and IM (2 mmol, 0.136 g) was added into the mixture and sonicated for 15 min to dissolve reagents. The vessel was sealed and stirred at 120 °C for 48 hr, then cooled back down to room temperature. The dark brown precipitate was collected using an external magnet, washed with ethanol and dried at 70 °C under vacuum.

## 2.6 | General procedure for the Knoevenagel condensation using Fe<sub>3</sub>O<sub>4</sub>/cellulose/Co-MOF as a catalyst

A mixture of various aldehydes (1 mmol), malononitrile (1.5 mmol) and Fe<sub>3</sub>O<sub>4</sub>/cellulose/Co-MOF (15 mg) was

stirred under solvent-free conditions at room temperature. Thin-layer chromatography (TLC) was utilized to monitor the progress of the reaction. After completion of the reaction, warm ethanol (10 ml) was added to the reaction mixture, Fe<sub>3</sub>O<sub>4</sub>/cellulose/Co-MOF was separated using a magnet and washed with ethanol. The solvent was evaporated and the solid was recrystallized from ethanol to produce the pure product. Then, the recovered catalyst was reused in five runs under similar conditions as the first run to exhibit the recyclability and stability of the prepared catalyst.

## 3 | RESULTS AND DISCUSSION

### 3.1 | Synthesis of Fe<sub>3</sub>O<sub>4</sub>/cellulose/co-MOF

The synthesis route of Fe<sub>3</sub>O<sub>4</sub>/cellulose/Co-MOF nanocomposite is displayed in Figure 1. First, Fe<sub>3</sub>O<sub>4</sub>/cellulose was fabricated through chemical modification of Fe<sub>3</sub>O<sub>4</sub> nanoparticles with cellulose in the presence of urea/NaOH. Pre-treating Fe<sub>3</sub>O<sub>4</sub> nanoparticles with

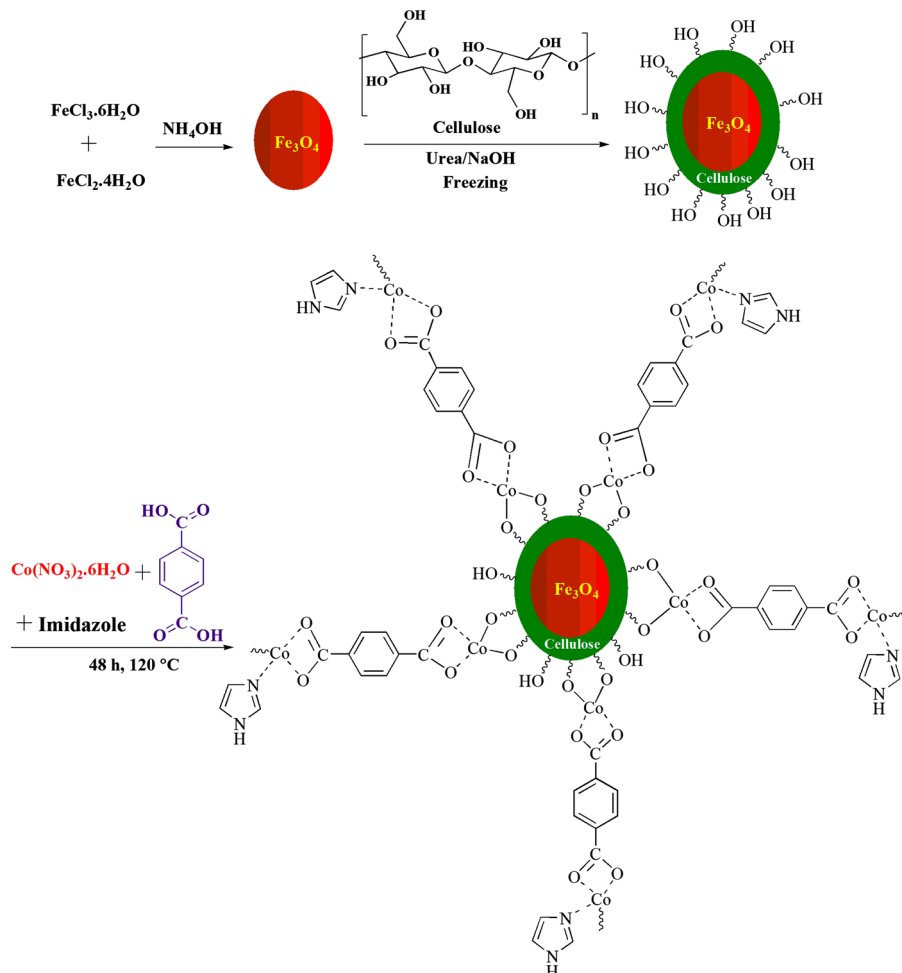


**FIGURE 1** Preparation of Fe<sub>3</sub>O<sub>4</sub>/cellulose/Co-MOF nanocomposite

cellulose was increased their compatibility toward Co-MOF and facilitated the growth of Co-MOF around  $\text{Fe}_3\text{O}_4$  nanoparticles. Second,  $\text{Fe}_3\text{O}_4$ /cellulose was treated with  $\text{Co}(\text{NO}_3)_2 \cdot 6\text{H}_2\text{O}$  (as an inorganic constituent), 1,4-BDC and IM (as organic linkers) and DMF (as a solvent) via heating to 120 °C for 48 hr to form  $\text{Fe}_3\text{O}_4$ /cellulose/Co-MOF nanocomposite. IM acts as a Lewis basic site and coordination regulator, and improve the catalytic performance of the fabricated nanocomposite. It is found that the combination of 1,4-BDC with IM generates a M-carboxylate coordination framework in which IM is coordinated as a neutral ligand.

### 3.2 | Characterization of the prepared compounds

Figure 2 displays the FT-IR spectra of  $\text{Fe}_3\text{O}_4$ ,  $\text{Fe}_3\text{O}_4$ /cellulose and  $\text{Fe}_3\text{O}_4$ /cellulose/Co-MOF. In the FT-IR spectrum of  $\text{Fe}_3\text{O}_4$ , the broad absorption band at 3465 cm<sup>-1</sup> corresponds to O-H stretching vibration in adsorbed  $\text{H}_2\text{O}$  molecules in  $\text{Fe}_3\text{O}_4$  nanoparticles and the peak observed at 582 cm<sup>-1</sup> is attributed to Fe-O stretching vibration. In the FT-IR spectrum of  $\text{Fe}_3\text{O}_4$ /cellulose, the two absorption peaks observed at 3552 and 3418 cm<sup>-1</sup> are related to the stretching vibrations of the O-H in cellulose, which became weaker and broader, implies the strong bonding between  $\text{Fe}_3\text{O}_4$  nanoparticles and cellulose molecules. The absorption peaks at 1449, 1163, 1116, 1034 and 615 cm<sup>-1</sup> implied the CH<sub>2</sub> symmetric scissoring in the pyranoid ring, C-O asymmetric bridge stretching, the

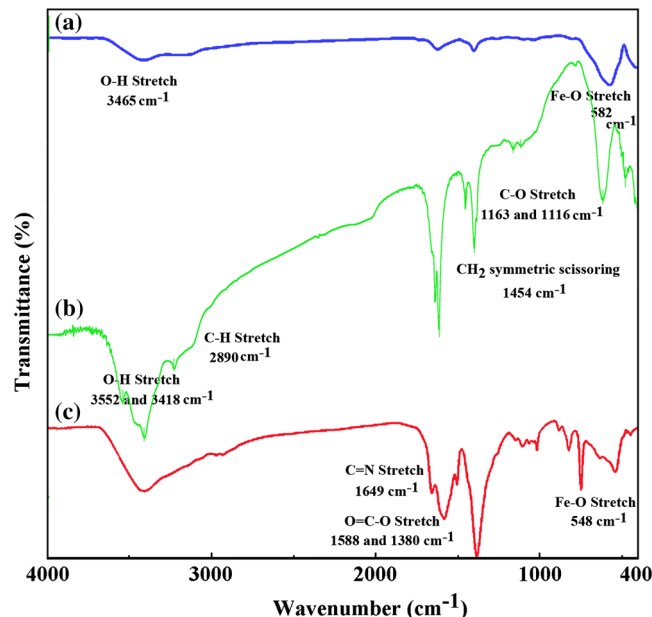


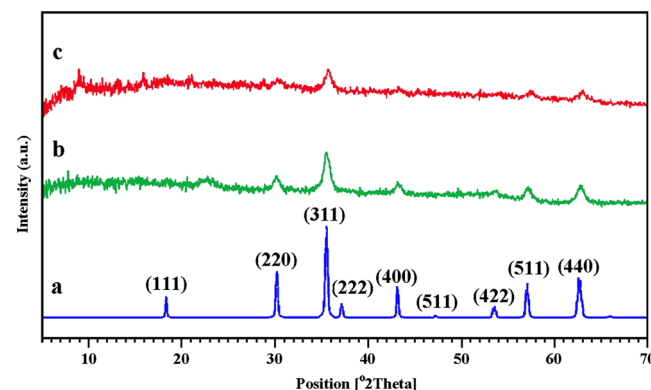
**FIGURE 2** FT-IR spectra of  $\text{Fe}_3\text{O}_4$  (a),  $\text{Fe}_3\text{O}_4$ /cellulose (b) and  $\text{Fe}_3\text{O}_4$ /cellulose/Co-MOF (c)

crystal absorption peak of cellulose, C-O-C pyranoid ring skeletal vibration and, the  $\beta$ -glycosidic units, respectively. The peak appeared at 548 cm<sup>-1</sup> in the spectrum of  $\text{Fe}_3\text{O}_4$ /cellulose/Co-MOF nanocomposite is attributed to Fe-O stretching vibration and the absorption peaks observed at 1588 and 1380 cm<sup>-1</sup> correspond to the asymmetric and symmetric stretching of the O=C-O bonded to Co.

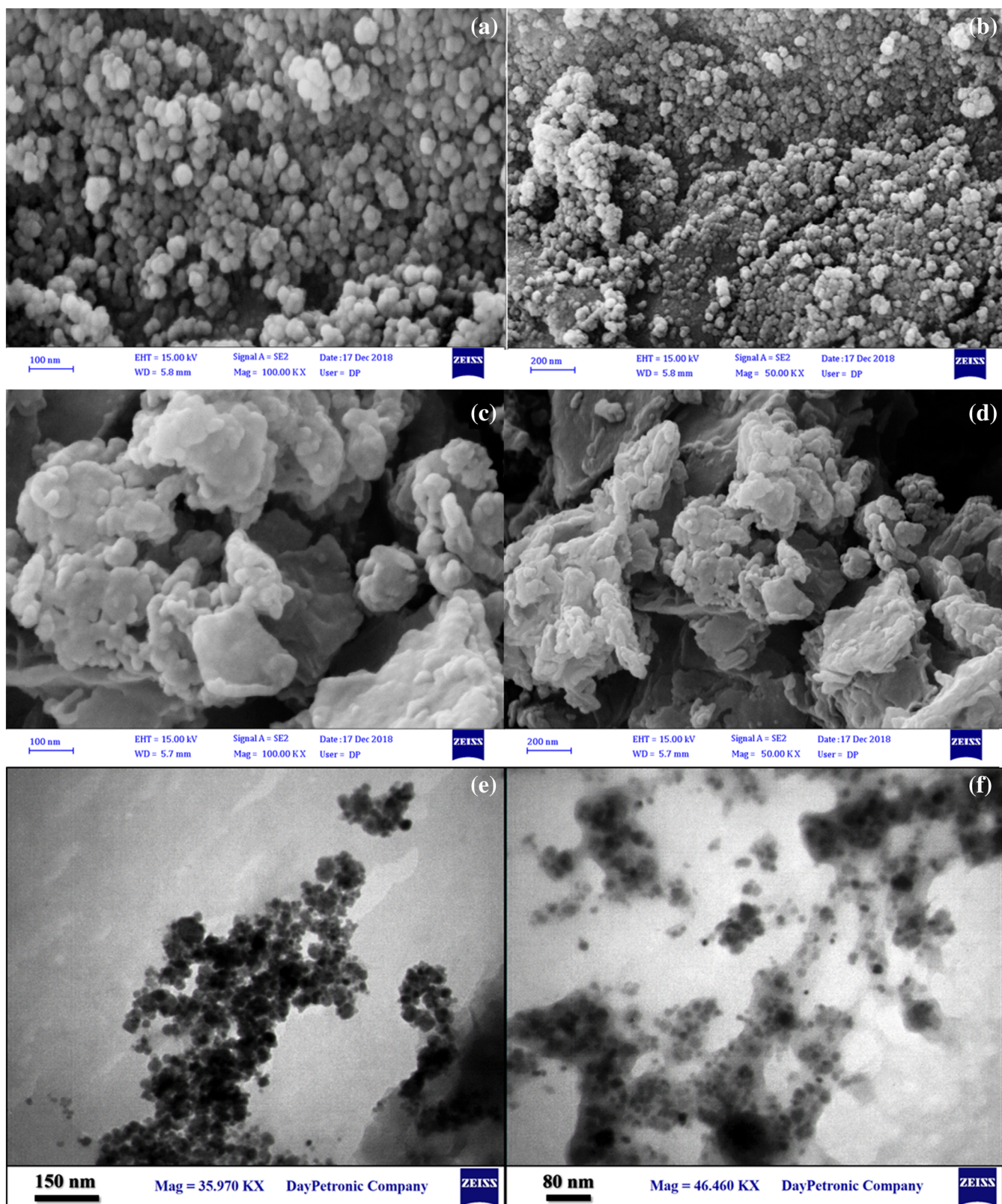
Figure 3 represents the XRD patterns of  $\text{Fe}_3\text{O}_4$  (a),  $\text{Fe}_3\text{O}_4$ /cellulose (b) and  $\text{Fe}_3\text{O}_4$ /cellulose/Co-MOF (c). It can be concluded by the XRD pattern of the  $\text{Fe}_3\text{O}_4$ /cellulose nanocomposite that it is almost similar in the crystal structure of  $\text{Fe}_3\text{O}_4$  nanoparticles after their congregation on the cellulose surface. The XRD pattern of  $\text{Fe}_3\text{O}_4$ /cellulose exhibits seven diffraction peaks at  $2\theta = 22.70, 30.5, 35.24, 43.20, 53.59, 57.13$  and  $62.76^\circ$ , ascribing to the crystal plane diffraction peaks of the (113), (220), (311), (400), (422), (511) and (440) of  $\text{Fe}_3\text{O}_4$  nanoparticles. The XRD pattern of  $\text{Fe}_3\text{O}_4$ /cellulose/Co-MOF displays that visible diffraction peaks at about  $2\theta = 8.95$  and  $15.88^\circ$  are assigned to the characteristic diffraction peaks of Co-MOF.

Figure 4 displays the FE-SEM images of  $\text{Fe}_3\text{O}_4$ /cellulose (a and b) and  $\text{Fe}_3\text{O}_4$ /cellulose/Co-MOF (c and d). As shown in the FE-SEM images of the  $\text{Fe}_3\text{O}_4$ /cellulose, the morphology of this material is spherical with uniform shapes and the average size of about 45 nm, while, the  $\text{Fe}_3\text{O}_4$ /cellulose/Co-MOF consists of cellulose fibers that Co-MOF particles with an average size of about 40 nm are dispersed on the surface of cellulose. The TEM analysis of  $\text{Fe}_3\text{O}_4$ /cellulose/Co-MOF shows the presence of Co-MOF on the cellulose surface (Figure 4 e and f).

The TGA/DTG analysis of  $\text{Fe}_3\text{O}_4$ /cellulose/Co-MOF is presented in Figure 5. As the results exhibited, initial TGA weight loss between 100 and 170 °C belongs to the removal of solvent and moisture from the framework. With the increasing temperature, it was stable up to 350 °C, with rapid weightlessness, which pointed out the



**FIGURE 3** XRD patterns of  $\text{Fe}_3\text{O}_4$  (a),  $\text{Fe}_3\text{O}_4$ /cellulose (b) and  $\text{Fe}_3\text{O}_4$ /cellulose/Co-MOF (c)



**FIGURE 4** FE-SEM images of Fe<sub>3</sub>O<sub>4</sub>/cellulose (a and b) and Fe<sub>3</sub>O<sub>4</sub>/cellulose/Co-MOF (c and d), TEM images of Fe<sub>3</sub>O<sub>4</sub>/cellulose/Co-MOF (e and f)

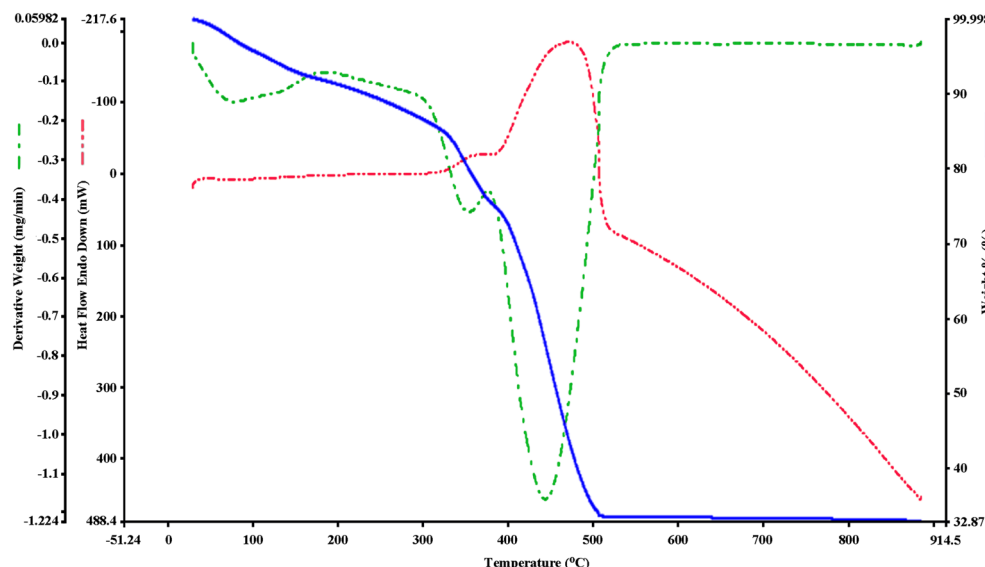


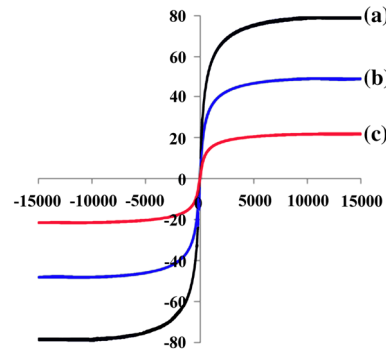
**FIGURE 5** STA thermogram of  $\text{Fe}_3\text{O}_4/\text{cellulose}/\text{Co-MOF}$

loss of organic matter was belong to leaving the final CoO. The final weightlessness occurred at  $450^\circ\text{C}$  signifying that the MOF structure began to collapse and decompose completely into oxides of Fe.

The magnetic properties of the materials were investigated by VSM. Magnetization curves of  $\text{Fe}_3\text{O}_4$  (a),  $\text{Fe}_3\text{O}_4/\text{cellulose}$  (b) and  $\text{Fe}_3\text{O}_4/\text{cellulose}/\text{Co-MOF}$  (c) are revealed in Figure 6. The magnetization curves exhibit a magnetic hysteresis loop. The saturation magnetization values were determined as 79.0, 48.0 and 21.5 emu/g for  $\text{Fe}_3\text{O}_4$  (a),  $\text{Fe}_3\text{O}_4/\text{cellulose}$  (b) and  $\text{Fe}_3\text{O}_4/\text{cellulose}/\text{Co-MOF}$  (c), respectively. Compared to the as-synthesized  $\text{Fe}_3\text{O}_4$  and  $\text{Fe}_3\text{O}_4/\text{cellulose}$ , the saturation magnetization of  $\text{Fe}_3\text{O}_4/\text{cellulose}/\text{Co-MOF}$  is reduced, but it still perseveres at a high level. Also the magnetic isolating of  $\text{Fe}_3\text{O}_4/\text{cellulose}/\text{Co-MOF}$  nanocomposite is tested by setting a magnet near the glass bottle of the nanocomposite.

In addition, the EDX analysis of the prepared catalyst confirms the existence of Co in the modified framework. It displays the presence of carbon, nitrogen, oxygen, Fe, and Co (Figure 7).

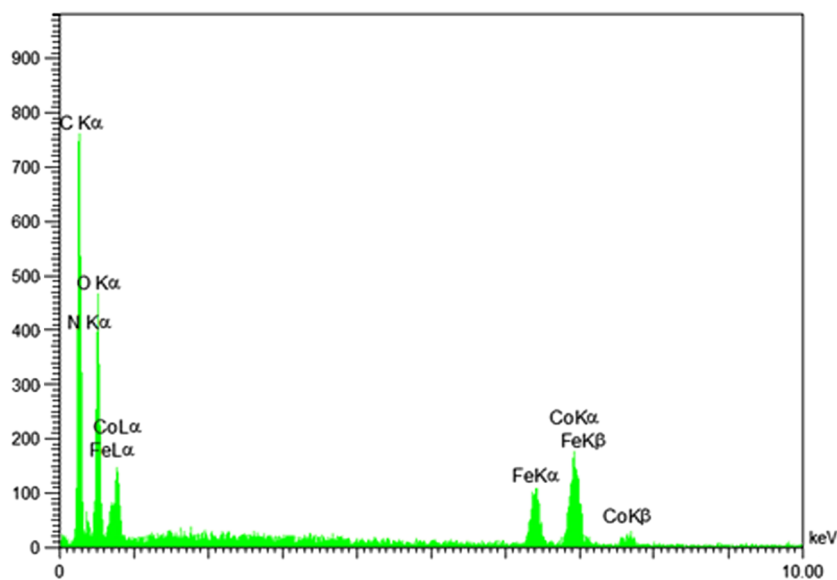
The porosity of  $\text{Fe}_3\text{O}_4/\text{cellulose}/\text{Co-MOF}$  is investigated by measuring nitrogen adsorption-desorption isotherms at 77 K.  $\text{Fe}_3\text{O}_4/\text{cellulose}/\text{Co-MOF}$  exhibits typical type IV isotherms with a hysteresis loop, designating its mesoporous feature. According to this analysis, the area of the surface, the total volume of the cavities and the mean diameter of the cavities were  $98 \text{ m}^2/\text{g}$ ,  $0.1309 \text{ cm}^3/\text{g}$  and  $5.0875 \text{ nm}$ , respectively. Furthermore,  $\text{Fe}_3\text{O}_4/\text{cellulose}/\text{Co-MOF}$  has a wide pore-size distribution from 1 to 60 nm, signifying the coexistence of structural pores in addition to interparticle pores.



**FIGURE 6** VSM analysis of  $\text{Fe}_3\text{O}_4$  (a),  $\text{Fe}_3\text{O}_4/\text{cellulose}$  (b) and  $\text{Fe}_3\text{O}_4/\text{cellulose}/\text{Co-MOF}$  (c)

### 3.3 | Catalytic activity test

The catalytic application of  $\text{Fe}_3\text{O}_4/\text{cellulose}/\text{Co-MOF}$  is examined in the Knoevenagel reaction under diverse conditions (Table 1). For the optimization of the reaction conditions, the reaction between malononitrile with benzaldehyde in the presence of  $\text{Fe}_3\text{O}_4/\text{cellulose}/\text{Co-MOF}$  as a catalyst is designated as a model reaction. The reaction progress is monitored by TLC. The model reaction is performed at 5, 10, 15 and 20 mg of  $\text{Fe}_3\text{O}_4/\text{cellulose}/\text{Co-MOF}$  loading. With increasing catalyst loading from 5 to 15 mg, the yield is enhanced and the best result in an appropriate time is obtained using 15 mg of catalyst (Table 1, entry 4). By increasing the catalyst loading to 20 mg no change in the yield of the product is observed (Table 1, entry 5). The effect of different solvents such as  $\text{H}_2\text{O}$ ,  $\text{EtOH}$ ,  $\text{CH}_2\text{Cl}_2$  and  $\text{CH}_3\text{CN}$  and solvent-free conditions is also investigated and the results reveal that  $\text{H}_2\text{O}$  and  $\text{EtOH}$  provide moderate yields (Table 1, entries 6 and

**FIGURE 7** EDS spectrum of Fe<sub>3</sub>O<sub>4</sub>/cellulose/Co-MOF**TABLE 1** Effect of catalyst loading and solvent in the Knoevenagel condensation of malononitrile with benzaldehyde

| $\text{C}_6\text{H}_5\text{CHO} + \text{HC}(=\text{CN})\text{CH}_2\text{CN} \xrightarrow[\text{Solvent, r.t.}]{\text{Catalyst}} \text{C}_6\text{H}_5\text{CH}(\text{CN})=\text{CH}_2\text{CN}$ |               |                                 |             |           |
|--|---------------|---------------------------------|-------------|-----------|
| Entry  | Catalyst (mg) | Solvent                         | Time (min.) | Yield (%) |
| 1  | -             | -                               | 240         | -         |
| 2  | 5             | -                               | 10          | 86        |
| 3  | 10            | -                               | 10          | 90        |
| 4  | 15            | -                               | 10          | 94        |
| 5  | 20            | -                               | 10          | 94        |
| 6  | 15            | H <sub>2</sub> O                | 10          | 68        |
| 7  | 15            | EtOH                            | 10          | 75        |
| 8  | 15            | CH <sub>2</sub> Cl <sub>2</sub> | 10          | 65        |
| 9  | 15            | CH <sub>3</sub> CN              | 10          | 55        |

Reaction conditions: benzaldehyde (1 mmol), malononitrile (1.5 mmol), catalyst (15 mg), room temperature.

7). Based on the obtained results the yields in H<sub>2</sub>O and EtOH solvents are lower than solvent-free conditions. It might be attributed to the solvation of the active functional groups by these solvents and hydrogen-bonding between active protonic sites of Fe<sub>3</sub>O<sub>4</sub>/cellulose/Co-MOF and these solvents which declines the catalytic efficiency. Hence, the use of 15 mg of the catalyst under the solvent-free conditions at room temperature is designated as optimum conditions. After the optimization of the conditions, the generality and the scope of this system are examined using several aromatic aldehydes bearing both

electron-donating and electron-withdrawing groups. Based on the obtained results all substrates give the corresponding products in relatively high yield in very short reaction time as reveal in Table 2. The benzaldehyde derivatives containing electron-withdrawing groups such as -NO<sub>2</sub>, and -Cl are transformed to the corresponding products with a high yield (Table 2, entries 2–4), whereas the benzaldehyde derivatives possessing electron-donating moieties including -OCH<sub>3</sub>, -CH<sub>3</sub>, and -OH provide the lower yields (Table 2, entries 5–7). This result proves that the benzaldehyde derivatives having electron-withdrawing groups are slightly reactive compared to those with electron-donating moieties. Additionally, the catalytic effect of Fe<sub>3</sub>O<sub>4</sub> and cellulose alone and Fe<sub>3</sub>O<sub>4</sub>/cellulose was investigated on the model reaction. It is observed that Fe<sub>3</sub>O<sub>4</sub> and cellulose alone could not catalyze the reaction efficiently and the product is obtained in low yields (44% and 32%) in long reaction times (6 and 12 hr). It is also found that Fe<sub>3</sub>O<sub>4</sub>/cellulose

**TABLE 2** The Knoevenagel condensation of several aromatic aldehydes with malononitrile in the presence of Fe<sub>3</sub>O<sub>4</sub>/cellulose/Co-MOF

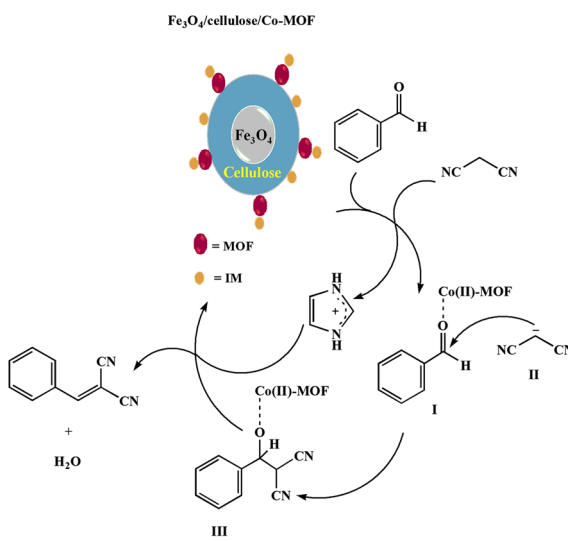
| Entry | R                 | Time (min) | Yield (%) |
|-------|-------------------|------------|-----------|
| 1     | H                 | 10         | 94        |
| 2     | 4-NO <sub>2</sub> | 8          | 97        |
| 3     | 4-Cl              | 10         | 98        |
| 4     | 2-Cl              | 45         | 97        |
| 5     | 4-MeO             | 15         | 88        |
| 6     | 4-Me              | 60         | 89        |
| 7     | 2-OH              | 15         | 78        |

Reaction conditions: aldehyde (1 mmol), malononitrile (1.5 mmol), catalyst (15 mg), room temperature.

provides the product in 53% yield for 8 hr. The experimental results show that Co-MOF is enhanced catalytic performance of modified  $\text{Fe}_3\text{O}_4$  nanoparticles.

The synthesized catalyst in this study has both Lewis acidic sites ( $\text{Co}^{2+}$ ) and basic sites (IM), hence it is an efficient heterogeneous catalyst for the Knoevenagel reaction. A mechanism for the  $\text{Fe}_3\text{O}_4$ /cellulose/Co-MOF-catalyzed Knoevenagel reaction of aldehyde and malononitrile was proposed (Scheme 1). Initially, the aldehyde is activated by  $\text{Co}^{2+}$  ion as a Lewis acid site (intermediate I). Uncoordinated IM adsorbed in Co-MOF serves as a base to promote the deprotonation of the methylene for the production of a carbanion intermediate (II). Next, the nucleophilic attack of the formed carbanion takes place on the activated carbonyl group. Lastly, the addition intermediate (III) can be rapidly converted to the benzylidene malononitrile after protonation and dehydration.<sup>[59]</sup>

In order to prove the heterogeneity of the catalyst, the filtration experiment of  $\text{Fe}_3\text{O}_4$ /cellulose/Co-MOF was performed. The catalyst was separated from the reaction



**SCHEME 1** Proposed mechanism for the Knoevenagel reaction catalyzed by  $\text{Fe}_3\text{O}_4$ /cellulose/Co-MOF

**TABLE 3** Comparison of the proposed catalyst with reported catalysts for the Knoevenagel condensation of benzaldehyde and malononitrile

| Catalyst                                  | Amount    | Time   | Solvent      | Temp. (°C) | Conversion (%) | Ref.     |
|---|-----------|--------|--------------|------------|----------------|----------|
| Au@Cu (II)-MOF                            | 19 mg     | 7 hr   | Toluene/MeOH | r.t.       | 99             | [60]     |
| $\text{Fe}_3\text{O}_4$ @ZIF-8            | 4 mol%    | 3 hr   | Toluene      | r.t.       | 94             | [61]     |
| ZIF-8                                     | 20 mg     | 3 hr   | Toluene      | r.t.       | 100            | [62]     |
| Amino-functionalized Zn-MOF               | 0.02 mmol | 6 hr   | Solvent-free | 60         | 99.9           | [54]     |
| Amino-functionalized Cd-MOF               | 0.02 mmol | 6 hr   | Solvent-free | 60         | 99.8           | [54]     |
| MOF-5                                     | 50 mg     | 48 hr  | Solvent-free | 25         | 99             | [59]     |
| $\text{Fe}_3\text{O}_4$ /cellulose/Co-MOF | 15 mg     | 10 min | Solvent-free | r.t.       | 94             | Our work |

mixture after 5 min, and the resulting filtrate was further stirred for 5 min. The conversion yield of the benzaldehyde remains unchanged for the filtrate even at extended time, indicating that the catalytic process is heterogeneous and there is not any progress for the reaction in the homogeneous phase.

### 3.4 | Reusability of $\text{Fe}_3\text{O}_4$ /cellulose/Co-MOF

To examine the reusability of  $\text{Fe}_3\text{O}_4$ /cellulose/Co-MOF, after the completion of the reaction, the catalyst is collected, separated, and then reused under similar conditions as the first run. This experiment is repeated five times and it is found that  $\text{Fe}_3\text{O}_4$ /cellulose/Co-MOF is stable under the applied conditions and can be reused at least five times without a considerable decreasing in its catalytic activity (Figure 8).

### 3.5 | Comparison of the proposed catalyst with the previously reported catalysts for the Knoevenagel condensation

The comparison between the performance of the Knoevenagel condensation based on the  $\text{Fe}_3\text{O}_4$ /cellulose/Co-MOF catalyst and some previously reported catalysts involving the Knoevenagel condensation is listed in Table 3. It is found that  $\text{Fe}_3\text{O}_4$ /cellulose/Co-MOF exhibits

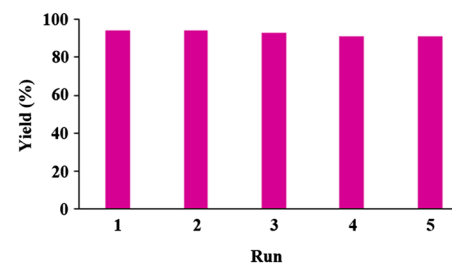


**FIGURE 8** Reusability of  $\text{Fe}_3\text{O}_4$ /cellulose/Co-MOF

advantages in terms of cost-effectiveness and simplicity, low temperature and very short reaction time. Additionally, it consumes very short reaction time and mild conditions in the Knoevenagel condensation compared with the literature.<sup>[44–46]</sup>

## 4 | CONCLUSIONS

In this study, the synthesis, characterization and catalytic application of Co-MOF-coated magnetic regenerated cellulose-coated nanoparticles were reported. The FTIR, EDX and STA analyses successfully confirmed the good immobilization and high stability of organic linkers (terephthalic acid and IM) and inorganic constituent (CO<sup>2+</sup>) onto the surface of Fe<sub>3</sub>O<sub>4</sub>. The SEM and TEM images exhibited that the Co-MOF particles are well dispersed on the surface of cellulose. The VSM technique displayed good magnetic properties for Fe<sub>3</sub>O<sub>4</sub>/cellulose/Co-MOF. The prepared novel nanocomposite was successfully applied as an effective heterogeneous catalyst in the Knoevenagel condensation for the synthesis of benzylidene malononitrile derivatives in high yields. The catalyst was easily recovered and reused without a significant decrease in activity. The other features of the present study include straightforward preparation of the catalyst, accomplishing reaction at room temperature, solvent-free media, low loading of catalyst and short reaction time. This work provides a combination of modified Fe<sub>3</sub>O<sub>4</sub> nanoparticles with MOF will be more powerful catalysts.

## ACKNOWLEDGEMENTS

We are grateful to Yasouj University for financial assistance.

## ORCID

Zahra Rafiee  <https://orcid.org/0000-0002-4296-8760>

## REFERENCES

- [1] D. Nunes, A. Pimentel, L. Santos, P. Barquinha, L. Pereira, E. Fortunato, R. Martins, R. Martins, *Metal oxide nanostructures synthesis, properties and applications*, Elsevier 2019.
- [2] X. Li, J. Wei, Q. Li, S. Zheng, Y. Xu, P. Du, C. Chen, J. Zhao, H. Xue, Q. Xu, H. Pang, *Adv. Funct. Mater.* **2018**, *28*, 1800886
- [3] H. Karimi-Maleh, O. A. Arotiba, *J. Colloid Interface Sci.* **2020**, *560*, 208.
- [4] H. Karimi-Maleh, M. Sheikhshoiae, I. Sheikhshoiae, M. Ranjbar, J. Alizadeh, N. W. Maxakato, A. Abbaspourrad, *New J. Chem.* **2019**, *43*, 2362.
- [5] M. Miraki, H. Karimi-Maleh, M. A. Taher, S. Cheraghi, F. Karimi, S. Agarwal, V. K. Gupta, *J. Mol. Liq.* **2019**, *278*, 672.
- [6] Z. Shamsadin-Azad, M. A. Taher, S. Cheraghi, H. Karimi-Maleh, *J. Food, Meas. Charact.* **2019**, *13*, 1781.
- [7] F. Talebi, Z. Rafiee, *Polym. Bull.* **2019**. In press
- [8] M. Rasekh, Z. Rafiee, *High Perform. Polymer* **2019**. In press
- [9] E. A. Campos, D. V. B. S. Pinto, J. I. S. de Oliveira, E. d. C. Mattos, R. d. C. L. Dutra, *J. Aerosp. Technol. Manag.* **2015**, *7*, 267.
- [10] H. Karimi-Maleh, M. Shafieizadeh, M. A. Taher, F. Opoku, E. M. Kiarii, P. P. Govender, S. Ranjbari, M. Rezapour, Y. Orooji, *J. Mol. Liq.* **2019**, *112040*.
- [11] H. Karimi-Maleh, C. T. Fakude, N. Mabuba, G. M. Peleyeu, O. A. Arotiba, *J. Colloid Interface Sci.* **2019**, *554*, 603.
- [12] E. Rahmati, Z. Rafiee, *New J. Chem.* **2019**, *43*, 8492.
- [13] S. Vaysipour, M. Nasr-Esfahani, Z. Rafiee, *Appl. Organomet. Chem.* **2019**, e5090.
- [14] A. Ali, H. Zafar, M. Zia, I. U. Haq, A. R. Phull, J. Sarfraz Ali, A. Hussain, *Nanotechnol. Sci. Appl.* **2016**, *9*, 49.
- [15] N. Zhu, H. Ji, P. Yu, J. Niu, M. U. Farooq, M. W. Akram, I. O. Udego, H. Li, X. Niu, *Nanomaterials* **2018**, *8*, 810.
- [16] S. Gui, X. Shen, B. Lin, *Rare Met.* **2006**, *25*, 426.
- [17] B. Kakavandi, A. J. Jafari, R. R. Kalantary, S. Nasseri, A. Ameri, A. Esrafily, *J. Environ. Health Sci. Eng.* **2013**, *10*, 19.
- [18] M. Muthiah, I. K. Park, C. S. Cho, *Biotechnol. Adv.* **2013**, *31*, 1224.
- [19] A. Maleki, M. Kamalzare, *Cat. Com.* **2014**, *53*, 67.
- [20] X. Zhao, H. Li, A. Ding, G. Zhou, Y. Sun, D. Zhang, *Mater. Lett.* **2016**, *163*, 154.
- [21] Q. Lu, Y. Zhang, H. Hu, W. Wang, Z. Huang, D. Chen, M. Yang, J. Liang, *Nanomaterials* **2019**, *9*, 275.
- [22] S. T. Meek, J. A. Greathouse, M. D. Allendorf, *Adv. Mater.* **2011**, *23*, 249.
- [23] H. C. Zhou, J. R. Long, O. M. Yaghi, *Chem. Rev.* **2012**, *112*, 673.
- [24] R. Zhu, J. Ding, L. Jin, H. Pang, *Coord. Chem. Rev.* **2019**, *389*, 119.
- [25] H. Furukawa, K. E. Cordova, M. O'Keeffe, O. M. Yaghi, *Science* **2013**, *341*, 1230444
- [26] S. Zheng, X. Li, B. Yan, Q. Hu, Y. Xu, X. Xiao, H. Xue, H. Pang, *Adv. Energy Mater.* **2017**, *7*, 1602733
- [27] M. Yousefian, Z. Rafiee, *Carbohydr. Polym.* **2020**, *228*, 115393
- [28] S. Zhu, J. Ge, C. Liu, W. Xing, *EnergyChem* **2019**, *1*, 100018.
- [29] Z. Zhao, J. Ding, R. Zhu, H. Pang, *J. Mater. Chem. A* **2019**, *7*, 15519.
- [30] Y. Zheng, S. Zheng, H. Xue, H. Pang, *Adv. Funct. Mater.* **2018**, *28*, 1804950
- [31] X. Xiao, L. Zou, H. Pang, Q. Xu, *Chem. Soc. Rev.* **2020**. <https://doi.org/10.1039/c7cs00614d>
- [32] S. Yuan, L. Feng, K. Wang, J. Pang, M. Bosch, C. Lollar, Y. Sun, J. Qin, X. Yang, P. Zhang, Q. Wang, L. Zou, Y. Zhang, L. Zhang, Y. Fang, J. Li, H. C. Zhou, *Adv. Mater.* **2018**, *1704303*
- [33] S. Gao, N. Zhao, M. Shu, S. Che, *Appl. Catal. A. Gen.* **2010**, *388*, 196.
- [34] C. Le Calvez, M. Zouboulaki, C. Petit, L. Peeva, N. Shirshova, *RSC Adv.* **2016**, *6*, 17314.
- [35] C. Lei, J. Gao, W. Ren, Y. Xie, S. Yassin, H. Abdalkarim, S. Wang, Q. Ni, J. Yao, *Carbohydr. Polym.* **2019**, *205*, 35.
- [36] X. Gao, G. Ji, R. Cui, Z. Liu, *Mater. Lett.* **2019**, *237*, 197.
- [37] F. M. Zhang, J. L. Sheng, Z. D. Yang, X. J. Sun, H. L. Tang, M. Lu, H. Dong, F. C. Shen, J. Liu, Y. Q. Lan, *Angew. Chem. Int. Ed.* **2018**, *57*, 12106.

- [38] F. Ke, L. G. Qiu, J. Zhu, *Nanoscale* **2014**, *6*, 1596.
- [39] A. Wojtaszek-Gurdak, V. Calvino-Casilda, A. Grzesinska, R. Martin-Aranda, M. Ziolek, *Microporous Mesoporous Mater.* **2019**, *280*, 288.
- [40] M. R. Shakil, A. G. Meguerdichian, H. Tasnim, A. Shirazi-Amin, M. S. Seraji, S. L. Suib, *Inorg. Chem.* **2019**, *58*, 5703.
- [41] A. Bahuguna, A. Kumar, T. Chhabra, A. Kumar, V. Krishnan, *ACS Appl. Nano Mater.* **2018**, *1*, 6711.
- [42] Y. Cui, J. Du, Y. Liu, Y. Yu, S. Wang, H. Pang, Z. Liang, J. Yu, *Polym. Chem.* **2018**, *9*, 2643.
- [43] X. He, J. Zhong, Z. Cao, J. Wang, F. Gao, D. Xu, *Prog. Org. Coat.* **2019**, *129*, 21.
- [44] D. Khan, S. Mukhtar, M. A. Alsharif, M. I. Alahmdi, N. Ahmed, *Tetrahedron Lett.* **2017**, *58*, 3183.
- [45] B. Voigt, A. Matviitsuk, R. Mahrwald, *Tetrahedron* **2013**, *69*, 4302.
- [46] R. A. Kudirka, R. M. Barfield, J. M. McFarland, P. M. Drake, A. Carlson, S. Banas, W. Zmolek, A. W. Garofalo, D. Rabuka, *ACS Med. Chem. Lett.* **2016**, *7*, 994.
- [47] Y. Ogiwara, K. Takahashi, T. Kitazawa, N. Sakai, *J. Org. Chem.* **2015**, *80*, 3101.
- [48] U. D. Joshi, P. N. Joshi, S. S. Tamhankar, V. V. Joshi, C. V. Rode, V. P. Shiralkar, *Appl. Catal. A* **2003**, *239*, 209.
- [49] J. F. Zhou, Y. Z. Song, J. S. Lv, G. X. Gong, S. Tu, *Facile One-Pot, Synth. Commun.* **2009**, *39*, 1443.
- [50] A. Das, N. Anbu, A. Dhakshinamoorthy, S. Biswas, *Microporous Mesoporous Mater.* **2019**, *284*, 459.
- [51] X. Han, Y. X. Xu, J. Yang, X. Xu, C. P. Li, J. F. Ma, *ACS Appl. Mater. Interfaces* **2019**, *11*, 15591.
- [52] N. Lolak, E. Kuyuldar, H. Burhan, H. Goksu, S. Akocak, F. Sen, *ACS Omega* **2019**, *4*, 6848.
- [53] K. Madasamy, S. Kumaraguru, V. Sankar, S. Mannathan, M. Kathiresan, *New J. Chem.* **2019**, *43*, 3793.
- [54] Z. W. Zhai, S. H. Yang, Y. R. Lv, C. X. Du, L. K. Li, S. Q. Zang, *Dalton Trans.* **2019**, *48*, 4007.
- [55] A. Karmakar, M. M. A. Soliman, E. C. B. A. Alegria, G. M. D. M. Rubio, M. F. C. Guedes da Silva, A. J. L. Pombeiro, *New J. Chem.* **2019**, *43*, 9843.
- [56] X. Wu, B. Wang, Z. Yang, L. Chen, *J. Mater. Chem. A* **2019**, *7*, 5650.
- [57] M. L. Gao, M. H. Qi, L. Liu, Z. B. Han, *Chem. Commun.* **2019**, *55*, 6377.
- [58] M. Mahdavi, M. B. Ahmad, M. J. Haron, F. Namvar, B. Nadi, M. Z. Ab Rahman, J. Amin, *Molecules* **2013**, *18*, 7533.
- [59] C. Guo, Y. Zhang, L. Zhang, Y. Zhang, J. Wang, *CrystEngComm* **2018**, *20*, 5327.
- [60] J. S. Wang, F. Z. Jin, H. C. Ma, X. B. Li, M. Y. Liu, J. L. Kan, G. J. Chen, Y. B. Dong, *Inorg. Chem.* **2016**, *55*, 6685.
- [61] A. Schejn, T. Mazet, V. Falk, L. Balan, L. Aranda, G. Medjahdi, R. Schneider, *Dalton Trans.* **2015**, *44*, 10136.
- [62] U. P. N. Tran, K. K. A. Le, N. T. S. Phan, *ACS Catal.* **2011**, *1*, 120.

**How to cite this article:** Zare E, Rafiee Z. Cellulose stabilized Fe<sub>3</sub>O<sub>4</sub> and carboxylate-imidazole and Co-based MOF growth as an exceptional catalyst for the Knoevenagel reaction. *Appl Organometal Chem.* 2020;e5516. <https://doi.org/10.1002/aoc.5516>